



Lawrence Berkeley Laboratory

UNIVERSITY OF CALIFORNIA

RECEIVED
LAWRENCE
BERKELEY LABORATORY

JUL 6 1984

LIBRARY AND
DOCUMENTS SECTION

Materials & Molecular Research Division

Submitted to Wear

ELEVATED TEMPERATURE COMBINED
EROSION-CORROSION OF STEELS

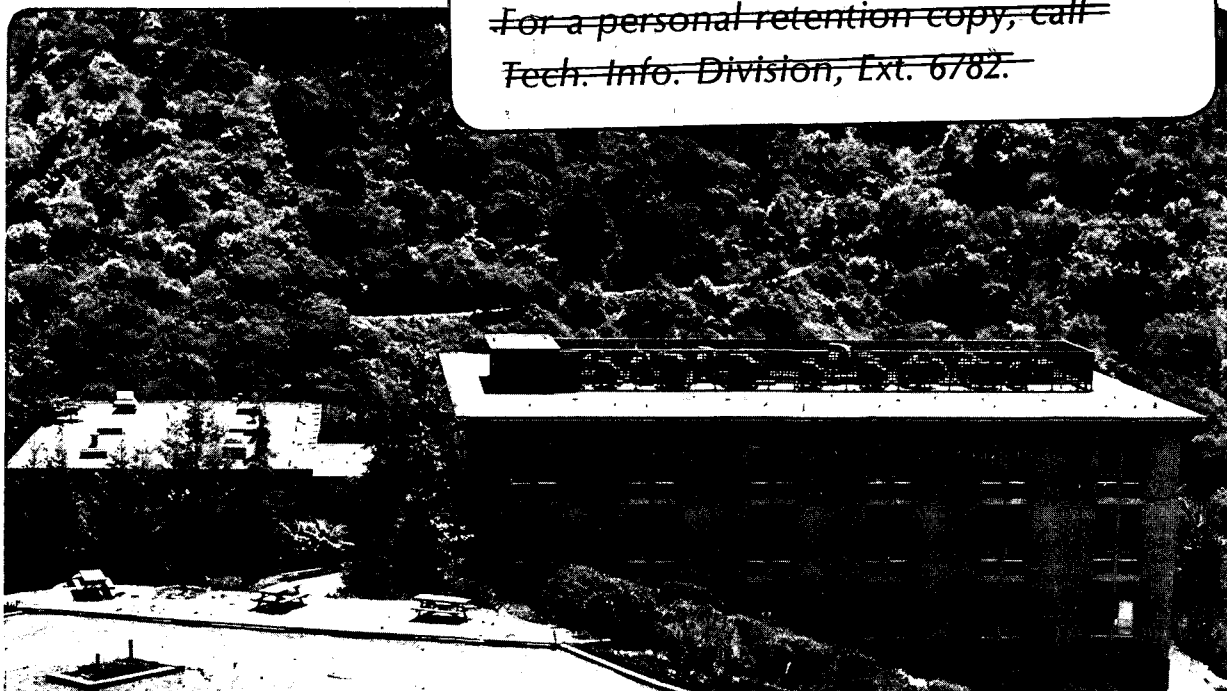
A. Levy, E. Slamovich, and N. Jee

April 1984

TWO-WEEK LOAN COPY

*This is a Library Circulating Copy
which may be borrowed for two weeks.*

~~For a personal retention copy, call
Tech. Info. Division, Ext. 6782.~~



LBL-17243
c.2

DISCLAIMER

This document was prepared as an account of work sponsored by the United States Government. While this document is believed to contain correct information, neither the United States Government nor any agency thereof, nor the Regents of the University of California, nor any of their employees, makes any warranty, express or implied, or assumes any legal responsibility for the accuracy, completeness, or usefulness of any information, apparatus, product, or process disclosed, or represents that its use would not infringe privately owned rights. Reference herein to any specific commercial product, process, or service by its trade name, trademark, manufacturer, or otherwise, does not necessarily constitute or imply its endorsement, recommendation, or favoring by the United States Government or any agency thereof, or the Regents of the University of California. The views and opinions of authors expressed herein do not necessarily state or reflect those of the United States Government or any agency thereof or the Regents of the University of California.



Lawrence Berkeley Laboratory

1 Cyclotron Road Berkeley, California 94720

(415) 486-4000 • FTS 451-4000

June 22, 1984

To: Recipients of LBL-17243

From: Technical Information Department, 90-2125

Re: Elevated Temperature Combined
Erosion-Corrosion of Steels, A. Levy,
E. Slamovich, and N. Jee, Lawrence Berkeley
Laboratory, University of California, Berkeley,
CA 94720, April, 1984

ERRATA-Particle velocity throughout this report
should be Vel.=5m/s, not 15m/s.

LBL 17243

ELEVATED TEMPERATURE COMBINED EROSION-CORROSION OF STEELS

Alan Levy, Elliott Slamovich and Nancy Jee
Lawrence Berkeley Laboratory
University of California
Berkeley, California 94720

Research sponsored by the Department of Energy under DOE/FEAA 15 10 10
0, Advanced Research and Technical Development, Fossil Energy Materials
Program, Work Breakdown Structure Element LBL-3.5 and under Contract
No. DE-AC0376SF00098.

ABSTRACT

An investigation was made of the effect of erodent particle size and test temperature on the combined erosion-corrosion behavior of a series of chromium containing steels containing 2 1/4, 5, 9, and 12% chromium. The particle sizes used were 5 μ m, 50 μ m, and 100 μ m and the test temperatures ranged from 800 $^{\circ}$ C to 950 $^{\circ}$ C (1470 - 1740 $^{\circ}$ F). The tests were made in the oxygen rich exhaust gases of a methane-air burner that propelled the particles at the specimens at 15m/s for 30 minutes.

It was determined that corrosion was the dominant mechanism at all test conditions for all alloys. The erosion process enhanced the growth rate of multi-layered iron oxide and iron-chromium oxide spinel scales and markedly changed the morphology of the scale surface and the thickness of the various scale layers. These changes were determined to be affected by the particle size of the erodent, the test temperature and the chromium content of the alloy.

INTRODUCTION

The ability of steel alloy surfaces to withstand the combined degradation modes of erosion and corrosion at elevated temperatures is an important consideration in the design of emerging coal conversion and utilization systems. Processes such as coal gasification and fluidized bed combustion can impose harsh environments on metal containment surfaces. Separate studies of the corrosion and erosion of various alloys in environments partially simulating those that occur in

process plants has been underway at this laboratory and several others for the past several years. Investigations of combined erosion-corrosion have also been conducted. The subject is an active research area at the present time.

High temperature corrosion research in both oxidizing and reducing atmospheres, with and without the presence of sulfur in the corrodant gas to simulate coal reaction products, has determined the nature and rates of formation of oxide and sulfide containing scales on chromium containing steel alloys.¹⁻⁸ The effects of important variables such as chromium content in the alloy, exposure temperature and time, and the composition of mixed reactant gases on the morphology, composition distribution and rates of formation of scale products have been determined. The effects of coal char reactant products from coal gasifiers in contact with alloy steels on their elevated temperature corrosion rates and mechanisms have been determined for a number of different char compositions and exposure conditions.⁹⁻¹¹

The erosion of metals in the absence of corrosion to determine the mechanisms of erosion have provided an understanding of how ductile metal surfaces deform and lose material from their surfaces.¹²⁻¹⁵ Separate studies of the erosion mechanisms of the scales formed on the surfaces of metals at elevated temperatures prior to carrying out the erosion tests at room temperature have provided some insight into how brittle scales on ductile metals erode in both thick and thin

layers.¹⁶⁻¹⁷ Studies have also been undertaken to determine the behavior of alloys subjected to the combined effects of erosion and corrosion in a single test.¹⁸⁻²⁰

Work in the field of erosion and corrosion has progressed to the point where observations of combined behavior can be partially interpreted in terms of the separate mechanisms which occur. In the work reported in this paper, this background has been used in an attempt to gain a more basic understanding of what is happening and how the characteristics of the alloys tested and the test conditions combine to produce the degradation products that are observed. However, the unexpected results of combined erosion-corrosion reported herein raise many questions that cannot be readily answered from the foundation research that is referred to above. It is hoped that more detailed study and interpretation of the corrosion and erosion phenomena reported in the references will result in detailed understanding of the behavior that will be discussed below.

TEST DESCRIPTION

The test specimens of each alloy (see Table 1 for composition) were exposed in the downstream duct of a methane-air burner operating with excess oxygen in the combustion gas. The exact partial pressure of oxygen was not determined. The specimens were 1.25cm on a side cubes with a small hole through their center for mounting on an alumina rod

that extended into the 10cm dia. duct perpendicular to its wall. The specimens were exposed so that two of their sides were at 45° angles to the exhaust gas and the other two sides were shielded from direct gas-particle impingement, thus providing two surfaces that were eroded-corroded and two surfaces that were only corroded on the same specimen. The ACES exhaust gas simulator at the Sandia Livermore National Laboratory Combustion Research Center was used for the tests.

The test conditions were:

- o gas oxygen rich methane-air combustion gas
- o velocity of particles 15 m/s
- o particles 5µm dia ave coal ash
50µm, 100µm dia ave Al₂O₃
- o solids loading 6g/min
- o test duration 30 minutes
- o impingement angle 45°
- o specimen temperature 700°-950°C
- o temperature differential across specimen 6°C

After the test exposure the specimens were cooled in less than 1 minute after the gas-particle flow was turned off to temperatures <300°C where further corrosion could not occur, removed and the exposed surfaces and cross sections microscopically analyzed using a scanning electron microscope (SEM).

RESULTS

Corrosion was the dominant mechanism of surface degradation at all of the test conditions investigated. The scales that formed and grew on the metal surfaces were affected by the impacting solid particles during their growth in several ways, depending upon the composition of the base alloy, the test temperature and the size of the erodent particles.

Reference 20 reports on the behavior of a series of chromium containing steels containing 0 to 18% chromium, all eroded with small, 5 μ m flyash particles. Analysis of the scale surface on all of the steels tested in that study indicates the presence of only iron oxide, Fe₂O₃⁽⁶⁾. Figure 1 shows the surface of the scale formed on the eroded-corroded side of 2 1/4Cr1Mo steel with the KEVEX peak analyses at several points that only show the presence of iron indicating only chromium free iron oxide.

Figure 2 shows the same condition existing at the surface for the 12Cr steel, 410SS. In Figure 2 both the corroded and eroded corroded sides of the same specimen are shown. KEVEX peak analyses No. 1 for each side show only the presence of iron oxide. KEVEX peak No. 2 for the corroded only side shows that particles of the flyash have been embedded in the small diameter iron oxide columns. The flyash is composed of oxides of magnesium, aluminum, silicon, potassium and calcium. The particles are slowed down considerably in the wakes on

the back sides of the specimens and can get caught in the scale.

The KEVEX peak no. 2 for the eroded-corroded side identifies a crystal of oxide that contains some chromium that is located somewhat below the average surface of the iron oxide columns. The location of the chromium is seen better in figure 3 which shows the cross sections of the scale formed on 410SS on both the corroded and eroded-corroded sides. The iron and chromium maps in the figure show that the scale formed is duplex with a top layer of iron oxide ($\alpha\text{-Fe}_2\text{O}_3$) and an underlayer of iron-chromium oxide spinel.⁽⁶⁾ The iron oxide layer on the eroded-corroded side of the specimen is thin compared to the iron oxide layer on the corroded side. The surface of the eroded-corroded side is made up of relatively large diameter columns of $\alpha\text{-Fe}_2\text{O}_3$ with void areas between them that extend down to the iron-chromium spinel layer. It is for this reason that there is a chromium peak in Figure 2 on the eroded-corroded side. Figure 4 shows that morphology of the corroded and eroded-corroded surfaces more clearly. The major differences that occurred in their morphology is one of the effects of combining erosion with the corrosion.

Figures 3 and 4 indicate that the erosion process significantly modifies the corrosion process. On the corroded only scale cross section in Figure 3, the small diameter, pointed columns of iron oxide shown in Figure 4 can be seen in cross section. On the eroded-corroded side of Figure 3 the large diameter columns of iron oxide shown in

seen in cross section.

The thickness of the upper and lower scale layers has been changed as a result of the erosion process. On the corroded only side of the specimen in Figure 3 both scale layers have approximately the same thickness. The contact zone between the lower scale layer and the substrate metal is intimate with no voids present. On the eroded-corroded side the thickness distribution between the upper, iron oxide layer and lower, iron-chromium oxide spinel layer is markedly different. The overall scale thickness is different on both sides. The large increase in the spinel layer on the eroded-corroded side apparently has depleted the substrate surface in chromium sufficiently to cause some Kirkendall type voids to occur at the scale-metal interface. The amount of voids between the upper and lower scales is near the same for both the corroded and eroded-corroded sides.

Effect of Particle Size

As the particle size of the erodent is increased, major changes occur in the morphology of the iron oxide scale surface. Figure 5 shows the surfaces of the erosion-corrosion side of 410SS eroded by 5 μ m flyash and 50 μ m and 100 μ m Al₂O₃. As the particle size increase from 5 μ m to 50 μ m dia particles, the diameter of the iron oxide columns decreases and the number increases. The type of column caused by the 50 μ m particles reverts to that which occurs on the corrosion side of

the specimens in the 5 μ m flyash test, figure 4. A further increase in particle size to 100 μ m dia Al₂O₃ causes a further major change in the topography of the scale surface, as can be seen in the lower photo in Figure 5. There are a minimum number of small nodules rising out of a cracked continuous iron oxide scale layer.

The variation in surface morphologies as a function of erodent particle size follows a pattern found in all of the other chromium containing steels tested. For example, Figure 6 shows the effect of erodent particle size on the surface scale morphology of the 5Cr 1/2Mo steel. Note that the magnification of the scale on the 100 μ m Al₂O₃ is one-third that of the two photos above it. A major change in the diameter and shape of the needles or blades formed on the erosion-corrosion surface occurred between the 5 μ m flyash and the 100 μ m Al₂O₃ tests. The 50 μ m dia particles resulted in a surface morphology that was similar to that found on the 410SS when it was eroded with 50 μ m dia particles, see Figure 5. This small diameter column morphology was found on almost all of the alloys that were eroded with 50 μ m dia particles.

The cross section of scales from tests using 100 μ m dia Al₂O₃ particles are shown in Figures 7 and 8. The scales were still multi-layered but differed significantly from those which occurred when 5 μ m flyash was used. In Figure 7 for 410SS, it can be seen that the overall thickness of the scale on the eroded-corroded side is much

greater than that which formed on the corrosion only side of the specimen (note the difference in magnification of the two photos). The erosion process markedly enhanced the growth of the scale.

The distribution of the iron oxide and iron-chromium oxide scale layers was changed between the eroded-corroded scale in the 5 μ m flyash test, Figure 3, and the 100 μ m Al₂O₃ test shown in Figure 7. The iron oxide, upper layer is now the thicker layer with not as much iron-chromium oxide spinel forming, relatively, as occurred in the 5 μ m flyash test. Small diameter voids occurred throughout the scale layers on the eroded-corroded side but did not occur on the corroded side.

There is also an internal scale layer that has formed on the eroded-corroded side, below the voids at the scale-metal interface that does not contain chromium. Based on evidence in reference 7, it is probably inward growing Fe₃O₄. The much smoother surface of the 100 μ m particle test scale compared to the 5 μ m particle test scale is also indicated in Figure 7.

Figure 8 shows the cross sections of the scales formed on the much lower chromium content 2 1/4Cr1Mo steel when 100 μ m particles were used at a lower test temperature than was used for the 410SS. The scale is essentially iron oxide. The chromium has concentrated in a thin iron-chromium oxide spinel layer at the scale-metal interface. The scale on the eroded-corroded side is significantly thicker than that on the corroded side, as occurred on 410SS. The scales that formed on both

sides of the specimen were almost completely separated from the substrate, indicating a strong susceptibility to spalling.

The consistent effect observed on all of the alloys for the eroding particles to increase the scale thickness on the erosion-corrosion side of the test specimen compared to the corrosion side was checked against the dynamic corrosion obtained by testing specimens in the flowing gases of the ACES burner without injecting any particles. Figure 9 compares the scales formed and their thicknesses for a number of test conditions. It can be seen by comparing the top two photos that static corrosion on the back side of the specimen and dynamic corrosion on the front side (gas flow without particles) results in nearly the same scale thickness with approximately a 10% increase on the dynamic corrosion side. This compares with a 60% increase in the scale thickness on the erosion-corrosion side when $5\mu\text{m}$ particles are used and a 345% increase when $100\mu\text{m}$ particles are used, all compared to the static corrosion side scale thickness.

Cross sections of the erosion-corrosion scales are seen in the lower two photos in Figure 9. The morphology of the static and dynamic corrosion scales are similar while there is a major difference in the two eroded-corroded scales in addition to their thickness difference. This seemingly anomalous behavior of the more erosive (larger size) particles causing markedly thicker scales to form was consistently observed for all of the chromium containing steels tested.

The differences in the morphology of the cross section and surface of three of the chromium containing steels tested at the same conditions are shown in Figure 10. These steels were eroded by 100 μ m Al₂O₃ particles. All three had iron oxide outer scales with the two higher chromium content steels having sizeable inner scales of iron-chromium oxide spinel.

The character of the surface of the outer scale differed for the three steels. The large, light particles on the surface of the 2 1/4Cr1Mo steel are alumina erodent particles that became embedded in the iron oxide scale. Note the difference in magnification between the three photos on the right side of Figure 10. The rosettes of iron oxide that formed on the 9Cr and 12Cr steels are completely different from the iron oxide morphology on the 2 1/4Cr1Mo Steel. The rosettes on the 410 steel are much larger than those which formed on the 9Cr1Mo steel (note the difference in magnification between the two photos). Similar rosettes of oxide scale are shown in reference 8.

In contrast with the differences in the eroded-corroded surfaces that were shown in Figure 10 when the erodent was 100 μ m Al₂O₃ the use of 50 μ m Al₂O₃ erodent particles resulted in a very similar surface scale morphology for the three alloys of varying chromium content shown in Figure 11. The columns of iron oxide with wrinkled and porous tops are similar in size and shape to the corroded side of the 410SS specimen that was tested with 5 μ m flyash, see Figure 4. The scale

morphologies of the three alloys shown in Figure 11 are completely different from their eroded-corroded surfaces when tested using either 5 μ m or 100 μ m size particles, see Figure 4 and 10. The cross sections of the three scales are multi-layered and have generally similar morphologies. The scale thickness of the 9Cr and 12Cr steels was thinner when the 50 μ m particles were used than when the 100 μ m particles were used as can be seen by comparing Figures 10 and 11 (note magnification differences).

Effect of Temperature

The morphology of the surface iron oxide scale was also affected by the test temperature when 5 μ m flyash and 100 μ m Al₂O₃ erodents were used, but not when 50 μ m Al₂O₃ particles were used. Figure 12 shows the changes that occurred on the 9Cr1Mo steel specimens when the temperature was varied from 800^o to 950^oC and 100 μ m size particles were used. The large diameter needles or blades that grew at 950^oC were very similar to those which grew at 800^oC on the 5Cr1/2Mo steel shown in Figure 6. The increase in the size of the microstructural elements with increasing temperature was expected, but the delicacy of some of the iron oxide crystals on surfaces that were being impacted by 100 μ m size particles as they were growing was unexpected.

Figure 13 shows the surfaces of the same alloy, 9Cr1Mo steel, at three different test temperatures when 50 μ m Al₂O₃ particles impacted the surface. As in the case of varying the chromium content shown in

Figure 11, varying the test temperature resulted in essentially the same type of microstructure for all three temperatures. The morphology was the same wrinkled, porous topped columns that were shown in Figure 11.

The effect of test temperature on the surface morphology of the alloys tested with the 5 μ m flyash particles was generally more dramatic in the differences that occurred. Figure 14 shows the surface of 410SS tested at 850 $^{\circ}$ and 950 $^{\circ}$ C on both the corroded and eroded-corroded surfaces. At the lower test temperature on the corroded side, some of the needle type crystals observed on the surface of the lower chromium content steels ⁽²⁰⁾ occurred. On the eroded-corroded side at the 850 $^{\circ}$ C test temperature, the needles have been removed and the remaining structure is essentially unaltered. Increasing the test temperature by 100 $^{\circ}$ C markedly changed the morphology of the surface of the iron oxide on both the corroded and eroded-corroded surfaces as can be seen on the right side photos in Figure 14.

Discussion

The major changes in the surface and cross section morphologies and compositions of the iron oxide base scales that formed on the chromium containing steels were unexpected. While there is some work in the literature that analyzes the growth of iron oxide and iron-chromium oxide spinels on the surfaces of chromium containing alloys,

6-8 the gross changes in morphology that were observed in this work, especially those that were promoted by the erosion process, have not been reported previously. Studying the high temperature corrosion literature referenced in the introduction only begins to account for the behavior reported therein.

Much work of interpretation and determination of mechanisms of the scales that formed must still be done. Hence, this discussion of the observed behavior will not be in depth at this time. Primarily, the work to date has identified phenomena that require more work to explain adequately.

The predominance of corrosion over erosion on the surfaces of ferritic steels with chromium contents up to 12% is due, at least in part, to the relatively high test temperatures used. These temperatures were selected to assure that scale would form at a rate that was compatible with a reasonable test time. Running the ACES burner at lower temperatures for extended periods of time was not technically or economically feasible. Generally, the test temperatures used were above the recommended service temperatures for the alloys tested. The erodent particle sizes and test velocities were representative of those which occur in coal gasification processes.

The occurrence of iron oxide, free of chromium, as the outer scale of a duplex or multi-layer scale structure with iron-chromium oxide spinel beneath the $\alpha\text{-Fe}_2\text{O}_3$ relates to several factors. Among them are

the partial pressure of oxygen at the scale-gas interface compared to that nearer the scale-metal interface, the short growth time of the scales, the difference in the outward diffusion rates of iron and chromium and their diffusion paths. Its occurrence on the higher chromium steels in this study as well as on the low chromium steels differs from the work reported in reference 8. However, the meticulous observations by Mitchell and his co-workers of the nucleation and growth of oxides on chromium containing steels in the temperature range 400°-950°C in reference 7,8 and in their other work promises to be a valuable aid in the effort that is being carried out to gain an understanding of how and why the scales reported on herein occurred in the manners that were observed.

The formation of needles, columns and rosettes or nodules of iron oxide on the surface is due to the manner in which iron diffuses upward and outward from oxide nuclei which form early in the oxidation process. It has been observed that the formations of needles are single crystals of $\alpha\text{-Fe}_2\text{O}_3$ as reported in reference 6. They grow from the tip upward as the result of fast diffusion paths along both their outside surfaces, and along the inner surface of tunnel walls that extend up the columns toward the tip. These surface short circuit diffusion paths are reported to be up to 9 times faster for iron than iron bulk diffusion in the $\alpha\text{-Fe}_2\text{O}_3$ and 4 times faster than grain boundary diffusion.⁶

In reference 7 Mitchell and co-workers describe the manner in which the oxides nucleate and grow in low (3%) and high (18%) chromium steels. He has postulated that the nuclei of the growth oxide crystals precipitate between a thin oxide film of uniform thickness that pre-exists on the metal surface before exposure to an elevated temperature and the metal surface itself. For low chromium content alloys, the nuclei grow upward and outward to become the iron oxide needles or columns observed herein. Rosettes are also formed such as those seen in Figure 10. Similar rosettes are shown in reference 8. For higher chromium content alloys, 9, 12, 18% Cr were reported, the nuclei are iron-chromium spinels and they grow inward.

The proposed mechanism of growth for the iron oxide is diagramed in reference 7. It entails surface diffusion of iron along the pre-existing oxide film to the nuclei sites. Once the nuclei have reached a critical size, no more nuclei are precipitated and the ones that are present grow laterally as well as upward until they impinge on adjacent ones. The keys to the formation of the nuclei which become the needles and columns of oxide appear to be the fast diffusion path of iron atoms along the interface of the pre-existing oxide and the protected location for nucleation between the pre-existing oxide film and the base metal.

Translating the mechanism in reference 7 to this study, on the corrosion side the pre-existing film remains relatively intact and the

iron can rapidly diffuse along it to many protected nuclei growth locations between the film and the base metal. Hence the columns formed are relatively small in diameter and many in number. On the erosion-corrosion side, the pre-existing oxide film is broken up by the early impacting erodent particles, permitting nucleation of oxide precipitates at relatively few sites where the oxide film was not struck and is still intact. These fewer nuclei can then grow to much larger diameter columns before they impinge on adjacent crystals. This mechanism could be the basis for the large differences between the size of the columns on the corroded side and on the eroded-corroded side of the test specimens.

For higher chromium content alloys, Mitchell included 9, 12 and 18% Cr steels in reference 7, inward growing iron-chromium oxide spinels are nucleated by the mechanism discussed above. While the study reported on herein found that the outer scale layer was always iron oxide, inner scales of iron-chromium oxide spinels were observed. These spinels, as reported in reference 7, 8, could be either $(\text{Fe,Cr})_3\text{O}_4$ or $\gamma\text{-(Fe,Cr)}_2\text{O}_3$. The light and dark areas shown in the inner, spinel scale layer for the 410SS in Figure 10 could be evidence that both spinels were present.

The significant increase in the thickness of the scale on the erosion-corrosion side of the test specimens compared to the corroded side and the change in the distribution of the iron oxide and the

spinel thicknesses between the corroded and eroded-corroded sides cannot be explained yet. They were a consistently occurring phenomena for all of the alloys tested with the degree depending on the composition of the alloy and the size of the eroding particles. The effects increased with increasing erodent particle size. Figure 3 shows a comparatively minor difference for 410SS when 5 μ m flyash was the erodent while Figure 7 shows a major difference when 100 μ m Al₂O₃ particles were used. An intermediate difference in the thickness is shown for the 2 1/4Cr1Mo steel in Figure 8. Also, the scales on the eroded-corroded side were thicker when 100 μ m erodent particles were used than when smaller particles were used. Compare Figures 10 and 11 for the 9Cr and 12Cr steels.

Dynamic corrosion tests were run on all of the test alloys and the results on 410SS, which are typical, are shown in Figure 9. The difference in scale thickness between the corroded and eroded-corroded sides of the same specimen was determined to not be due to dynamic corrosion effects. The ability of the impacting erodent particles to increase the growth rate of the oxide scale without removing it was demonstrated.

A key measurement that has not been successfully made accurately to date is the recession of the metal face beneath the scale. This is a difficult measurement to make because conventional markers such as platinum can be eroded off the surface during the test. It is,

therefore, not known whether the scale growth rate is more rapidly removing base metal or is building up a protective ceramic oxide barrier to impede metal loss.

In the presence of chromium, the formation of $Fe_{1-x}O$ at the metal interface is suppressed and, instead Fe_3O_4 forms.⁷ In Figure 6, beneath the iron-chromium spinel scale and next to the base metal, another layer of scale can be seen that does not contain any chromium and, hence, is probably Fe_3O_4 . The Fe_3O_4 that forms in the nuclei that grow into needles or columns is transformed to αFe_2O_3 sometime during the growth process.^{7, 8}

The description of the formation of a multi-layer scale on Fe-3% Cr steel by Mitchell in reference 8 matches perfectly with the scale on 2 1/4Cr1Mo steel on the corroded side shown in Figure 8. He described an inner, thin layer of (Fe, Cr) $3O_4$ spinel, a thicker, compact middle layer of Fe_3O_4 and a thin outer layer of αFe_2O_3 . Since positive identification of each scale layer was made by Mitchell and he identified a distinct layer of Fe_3O_4 , it is assumed that layers of Fe_3O_4 are present on some of the other lower chromium content steels, in addition to the scale shown in Figure 8, that are reported on herein. To date, only SEM X-ray maps of the principal elements present have been used in this study to aid in the identification of scales.

In reference 8 Mitchell reported the occurrence of considerable porosity in the oxide scales. He observed that more and smaller

diameter pores occurred in the higher chromium content alloys. The same observation was made in this study, but primarily in the scale on the erosion-corrosion side of the specimens. Compare Figure 7 of 410SS with Figure 8 of 2 1/4Cr 1Mo steel.

The effect of the test temperature on the surface morphology of the scales on the erosion-corrosion sides of the specimens was very pronounced when 5 μ m and 100 μ m particles were used as the erodent, Figure 12 and 14, but caused very little change when 50 μ m particles were used, Figure 13. The reason for this apparent anomaly is not known.

CONCLUSIONS

1. Corrosion is the dominant mechanism at all test conditions in the erosion-corrosion of chromium containing steels at temperatures from 700 $^{\circ}$ C-950 $^{\circ}$ C.
2. The erosion process enhances the growth of oxide scales.
3. The erosion process markedly changes the morphology and composition distribution of the oxide scales.
4. The morphology of the surface oxides are changed as the erodent particle size and test temperatures are changed.
5. Iron oxide (α -Fe₂O₃) forms as the outer scale in a multi-layer scale on all of the chromium containing steels tested. The inner

scale layers consist of iron-chromium oxide spinels and Fe_3O_4 , depending on the chromium content of the alloy.

6. Dynamic corrosion is not a contributor to the increase in the scale thickness on the erosion-corrosion sides of the test-specimens, compared to the corrosion side.
7. Larger erodent particles result in thicker scales.

ACKNOWLEDGMENT

Research sponsored by the U.S. Department of Energy under DOE/FEAA 15 10 10 0, Advanced Research and Technical Development, Fossil Energy Materials Program, Work Breakdown Structure Element LBL-3.5 and under Contract No. DE-AC03-76SF00098.

REFERENCES

1. Natesan, K., "Corrosion Behavior of Materials in Low and Medium BTU Coal Gasification Environments", Proceedings, NACE Conference on Corrosion-Erosion-Wear of Materials in Emerging Fossil Energy Systems, P 100-126, Berkeley, CA, January, 1982.
2. Perkins, R.A., Morse, G., Coors, W.C., "Materials for Syngas Coolers", EPRI AP-2518, Final Report, August, 1982, EPRI 3412 Hillview Avenue, Pal Alto, CA 94304.
3. Whittle, D.P. and Hindam, H., "Microstructure and Growth of Protective Cr_2O_3 and Al_2O_3 Scales at High Temperature", Proceedings, NACE Conference on Corrosion-Erosion-Wear of Materials in Emerging Fossil Energy Systems, p 54-99, Berkeley, CA, January, 1982.
4. Birks, N. and Meier, G., "Mechanism of Corrosion in Multiple Component Gases at High Temperatures", Proceedings, NACE Conference on Corrosion-Erosion-Wear of Materials in Emerging Fossil Energy Systems, p 1-53, Berkeley, CA, January 1982.
5. Hill, V.L. and Humphreys, B.A., "Mechanism of Corrosion of Structural Alloys in Coal Conversion Atmospheres", Proceedings, ASM Conference on The Properties and Performance of Materials in the Coal Gasification Environment, p 257-288, Pittsburgh, PA, September, 1980.
6. Voss, D.A., Butler, E.P., Mitchell, T.E., "The Growth of Hematite Blades During the High Temperature Oxidation of Iron", Met. Trans.A, V13A, p 929-935, May, 1982.
7. Kuroda, K., Labun, P.A., Welsch, G., Mitchell, T.E., "Oxide-Formation Characteristics in the Early Stages of Oxidation of Fe and Fe-Cr Alloys", Oxidation of Metals, v. 19 no. 3/4, p 117-127, 1983.
8. Kuroda, K., Labun, P.A., Welsch, G., Mitchell, T.E., "Microstructural Studies of the Oxidation of Fe-Cr Alloys", Proceedings JIMIS-3, High Temperature Corrosion Transactions of the Japan Institute of Metals, Supplement, 1983.
9. Foerster, T.F.W., Levy, A.V., Newman, J.S., "Corrosion of Metals in Coal Char Environments", NACE International Corrosion Conference Series no. 6, P 354-362, San Diego, CA, March, 1981.

10. Douglass, D.L., Bhide, V.S., Vineberg, E., "The Corrosion of Some Superalloys in Contact with Coal Chars in Coal Gasifier Atmospheres", *Oxidation of Metals*, v. 16, nos. 1/2, p 29-80, August, 1981.
11. Silence, W.L., Hill, V.L., Vesely, E.J., "The Effects of Environmental Variables on the Erosion-Corrosion Behavior of Candidate Materials for Coal Conversion Plants", *Proceedings ASM Conference on The Properties and Performance of Materials in the Coal Gasification Environment*, p 629-694, Pittsburgh, PA, September, 1980.
12. Levy, A., "The Erosion of Metal Alloys and Their Scales", *Proceedings NACE Conference on Corrosion-Erosion-Wear of Materials in Emerging Fossil Energy Systems*, P 298-376, Berkeley, CA, January, 1982.
13. Quadir, T and Shewmon, P., "Solid Particle Erosion Mechanisms in Copper and Two Copper Alloys", *Met. Trans. A*, v. 12A, p 1163-1176, July, 1981.
14. Emiliani, M. and Brown, R., "Erosion of Ti 6Al-4V by Spherical Silica Particles at 90° Impact Angle", *Proceedings of 6th International Conference on Erosion by Liquid and Solid Impact*, p 48-1, Cambridge University, Cambridge, England, September, 1983.
15. Cousens, A.K. and Hutchings, I.M., "A Critical Study of the Erosion of an Aluminium Alloy by Solid Spherical Particles at Normal Impingement", *Proceedings of ASME Conference on Wear of Materials 1983*, p 382-389, Reston, VA, April, 1983.
16. Zambelli, G. and Levy, A.V., "Particulate Erosion of NiO Scales", *Wear* v. 68 no. 3, p 269-288, May, 1981.
17. Maasberg, J.A. and Levy, A.V., "Erosion of Elevated Temperature Corrosion Scales on Metals", *Wear* v. 73 no. 2., p 355-370, November, 1981.
18. Schaefer, A.O. and Veseley, E. Jr., "MPC 4.4 Erosion-Corrosion of Materials in Coal Gasification Pilot Plants", *The Metal Properties Council Subcommittee 9 Report on Materials for Coal Conversion, 1982 Annual Report*, Metal Properties Council, Inc., 345 East 47th Street, New York, New York 10017, March, 1983.

19. Nagarajan, V. and Wright, I.G., "Influence of Oxidation Scales on High Temperature Corrosion-Erosion Behavior of Alloys", Proceedings of NACE Conference on High Temperature Corrosion, p 398-405, San Diego, CA, March, 1981.
20. Levy, A.V., and Slamovich, E., "Combined Corrosion-Erosion of Steels in Oxidizing Environments", Paper no. 84, NACE Corrosion 84, New Orleans, LA, April, 1984.

Figures

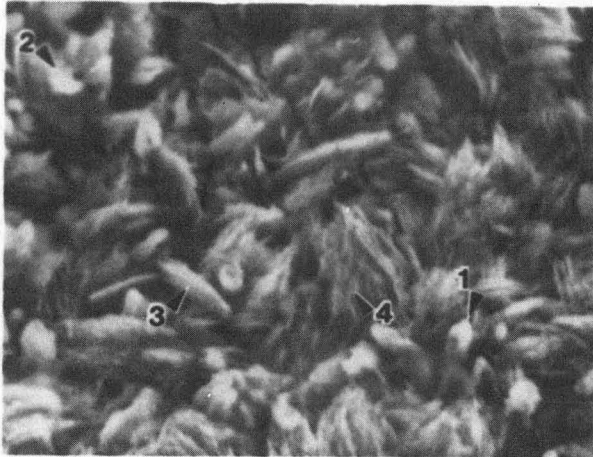
- Fig. 1. Peak analyses of composition of needle shape surface scale of 2 1/4Cr1Mo steel on eroded-corroded surface after 810°C test.
- Fig. 2. Peak analyses of composition of surface scales on 410SS after 950 °C test.
- Fig. 3. Cross section of 410SS scales formed at 950°C
- Fig. 4. Surface morphology of scale on 410SS formed at 950°C.
- Fig. 5. Morphology of surface scale on 410SS eroded by 5µm, 50µm, 100µm, particles.
- Fig. 6. Morphology of surface scale on 5Cr1/2Mo Steel eroded by 5µm, 50µm, 100µm particles.
- Fig. 7. Cross section of scales on 410SS from 100µm Al₂O₃ tests at 950°C.
- Fig. 8. Cross section of scales on 2 1/4Cr1Mo Steel from 100µm Al₂O₃ tests at 850°C.
- Fig. 9. Cross section of scales formed on 410SS at 950°C at different test conditions.
- Fig. 10. Cross section and surface morphology of scales of 2 1/4, 9 and 12Cr steels eroded-corroded at 850°C using 100µm Al₂O₃.
- Fig. 11. Cross section and surface morphology of scales of 5,9 and 12Cr steels eroded-corroded at 950°C using 50µm Al₂O₃.
- Fig. 12. Surface morphology of eroded-corroded 9Cr1Mo Steel at three different test temperatures using 100µm Al₂O₃.
- Fig. 13. Surface morphology of eroded-corroded 9Cr1Mo steel at three different test temperatures using 50µm Al₂O₃.
- Fig. 14. Surface morphology of eroded-corroded 410SS steel at two test temperatures using 5µm flyash.

TABLE 1

ALLOY COMPOSITION (NOMINAL)

ALLOY

	Cr	Ni	Mo	Si	Mn	C	P/S(max)	Fe
2 1/4Cr 1Mo	2.2		0.9	0.3	0.4	0.2	0.02	bal
5Cr 1/2Mo	5.1		0.6	0.02	0.5	0.1	0.02	bal
9Cr 1Mo	9		1.0	0.5	0.5	0.15	0.02	bal
410SS	12			1.0	1.0	0.2	0.1	bal



2 1/4 Cr 1 Mo Steel

Emersion Tester
Erosion-Corrosion
5 μ m flyash
Methane-air

Temp. = 810°C
Vel. = 15m/s
 α = 45°
Time = 30min.

2 μ m

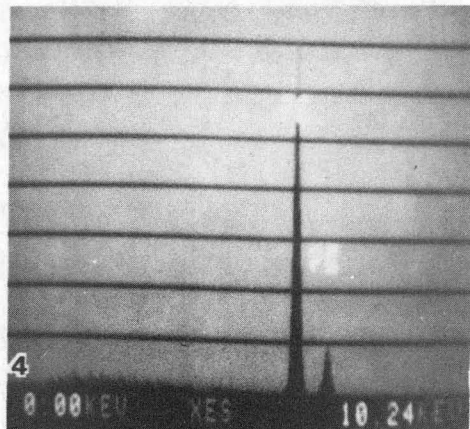
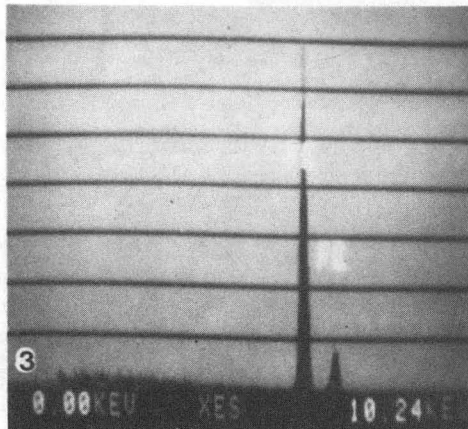
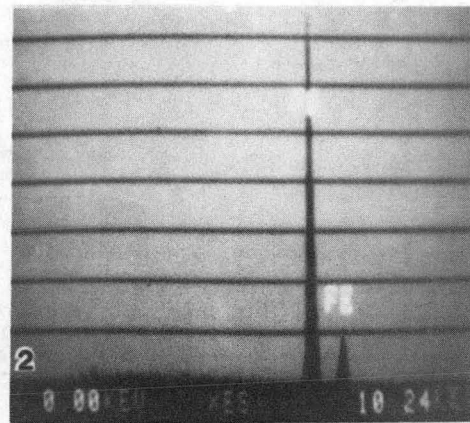
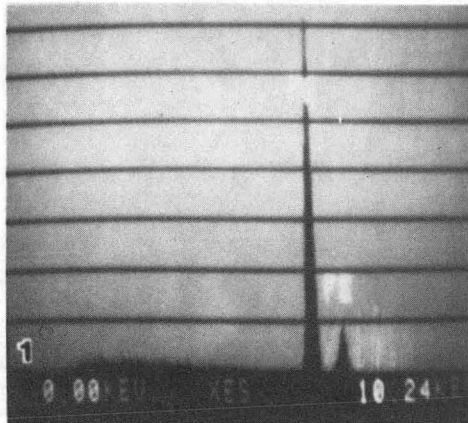
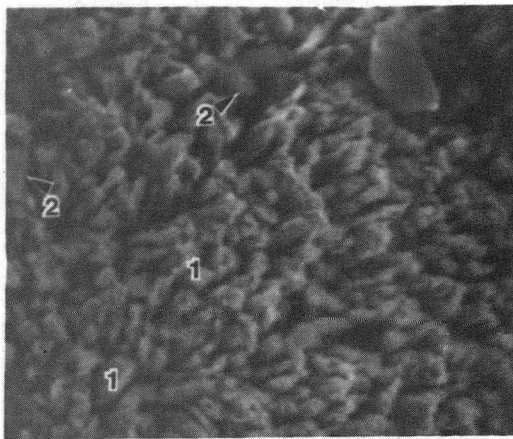
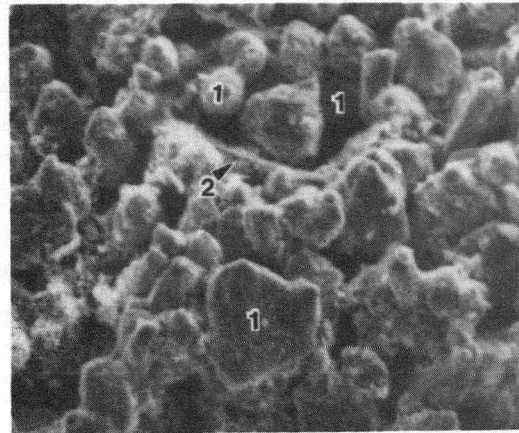


Fig. 1. Peak analyses of composition of needle shape surface scale of 2 1/4Cr1Mo steel on eroded-corroded surface after 810°C test.
XBB 841-102



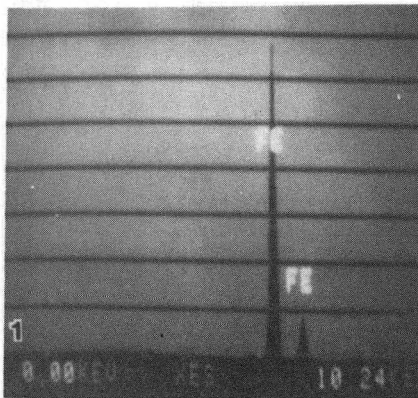
Corrosion

5µm



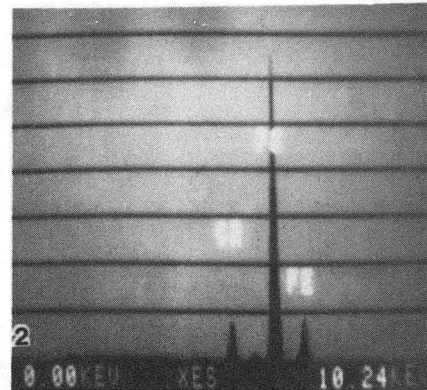
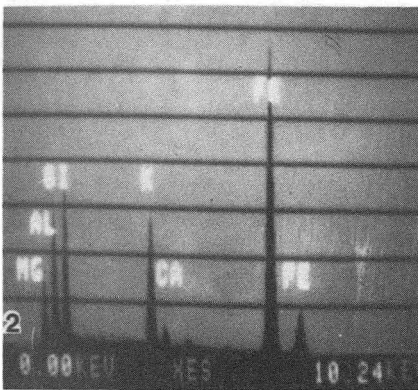
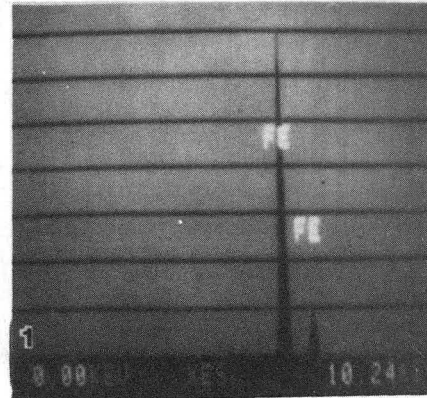
Erosion-Corrosion

2µm



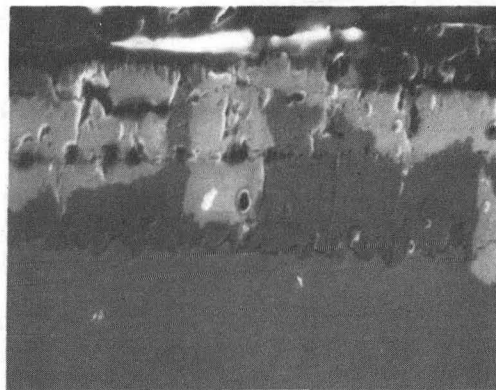
410 SS
Emersion Tester
5µm flyash
Methane-air

Temp. = 950°C
Vel. = 15m/s
α = 45°
Time = 30min.



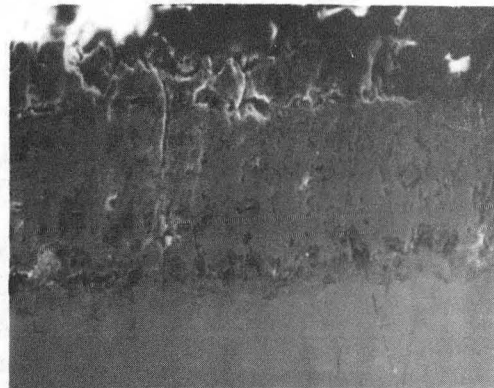
XBB 841-107A

Fig. 2. Peak analyses of composition of surface scales on 410SS after 950°C test.



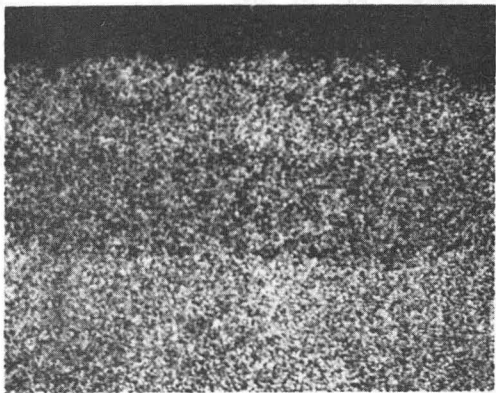
Corroded

20µm

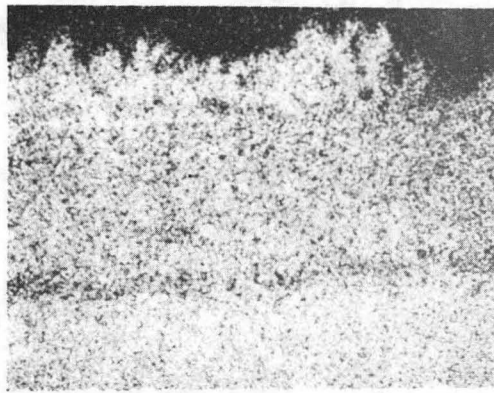


Eroded-Corroded

20µm



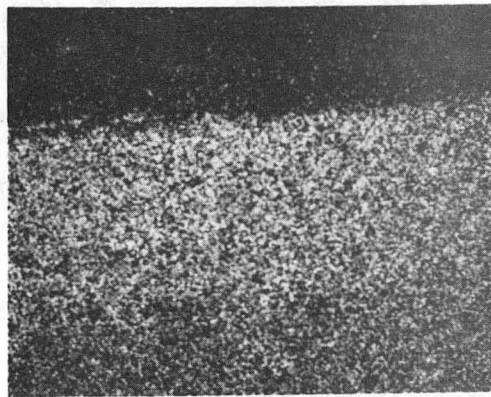
Fe Map



Fe Map



Cr Map

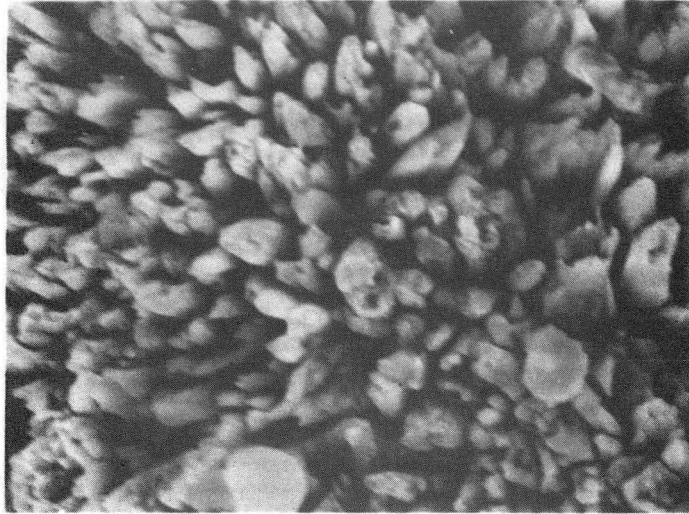


Cr Map

410 SS
 Emersion Tester
 5µm flyash
 Methane-air
 Temp. =950°C
 Vel. =15m/s
 α =45°
 Time =30min.

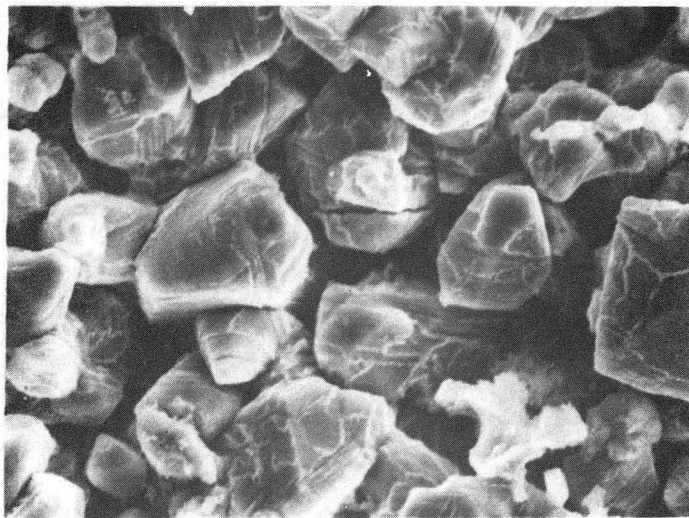
XBB 833-1827

Fig. 3. Cross section of 410SS scales formed at 950°C.



Corroded

3 μ m



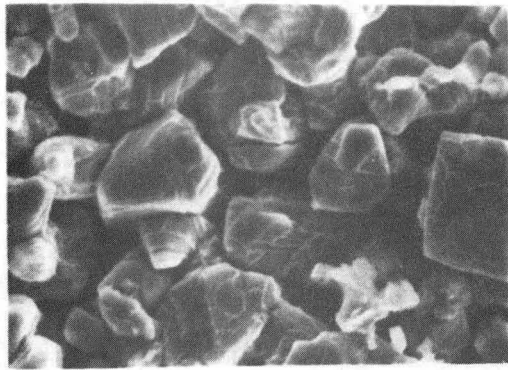
Eroded-Corroded

8 μ m

410 SS

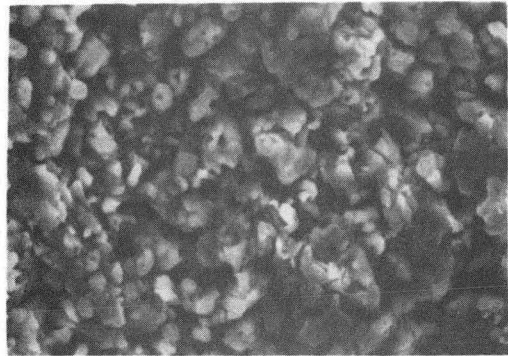
Emersion Tester	Temp. =950°C
5 μ m flyash	Vel. =15m/s
Methane-air	" =45°
	Time =30min

Fig. 4. Surface morphology of scale on 410SS formed at 950°C. XBB 841-101



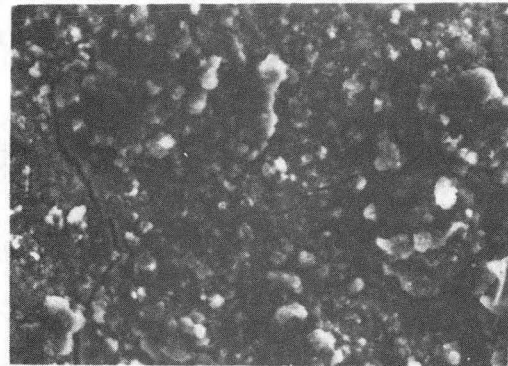
5µm flyash

5µm



50µm Al₂O₃

3µm



100µm Al₂O₃

15µm

410 SS

Emersion Tester Temp. =950°C
Erosion-Corrosion Vel. =15m/s
Methane air α =45°
Time =30min.

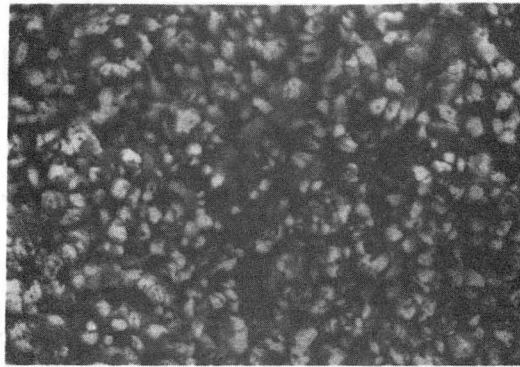
XBB 841-103

Fig. 5. Morphology of surface scale on 410SS eroded by 5µm, 50µm and 100µm particles.



5µm flyash

2µm



50µm Al₂O₃

3µm



100µm Al₂O₃

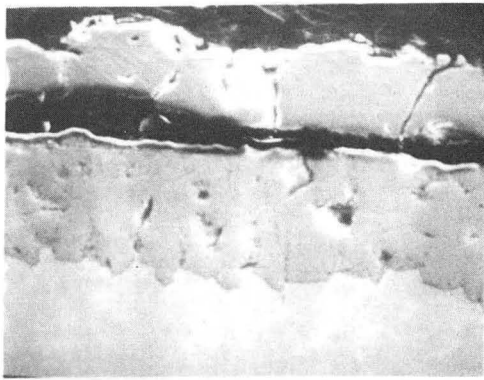
10µm

5 Cr 1/2 Mo Steel

Emersion Tester Temp. =800°C
Erosion-Corrosion Vel. =15m/s
Methane air α =45°
Time =30min.

Fig. 6. Morphology of surface scale on 5Cr1/2Mo steel eroded by 5µm, 50µm, 100µm particles.

XBB 841-100



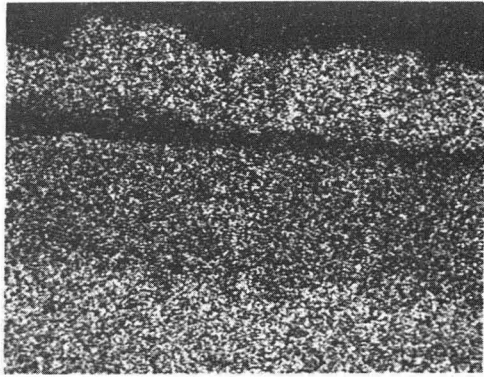
Corroded

15µm

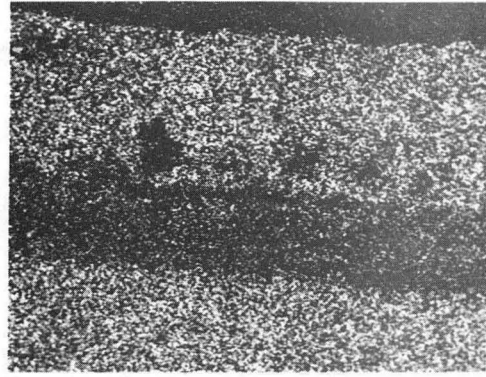


Eroded-Corroded

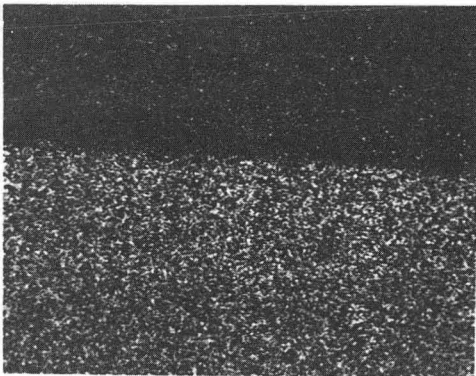
50µm



Fe Map



Fe Map



Cr Map



Cr Map

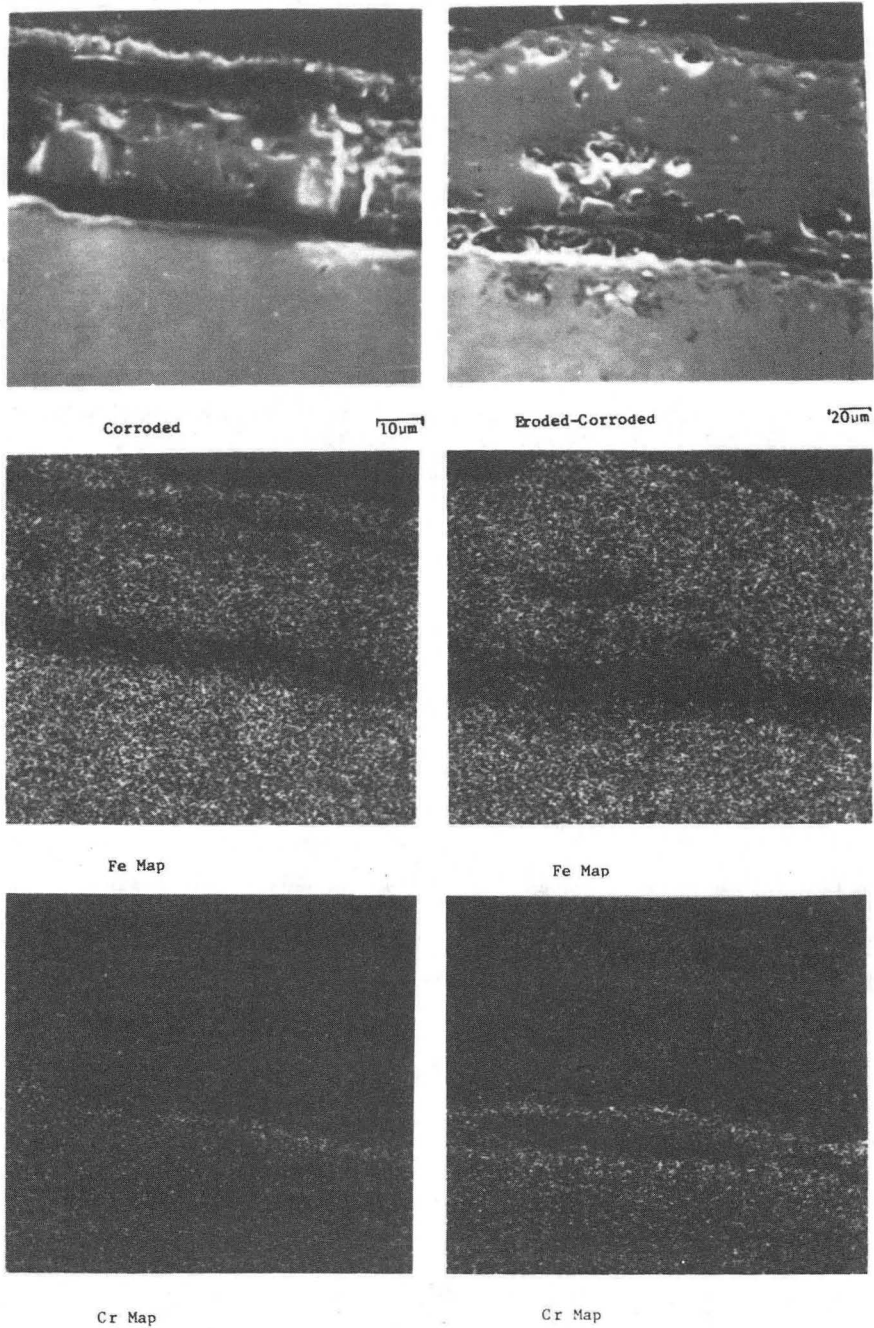
XBB 837-6107

410 SS

Emersion Tester
100µm Al₂O₃
Methane-air

Temp. =950°C
Vel. =15m/s
α =45°
Time =30min.

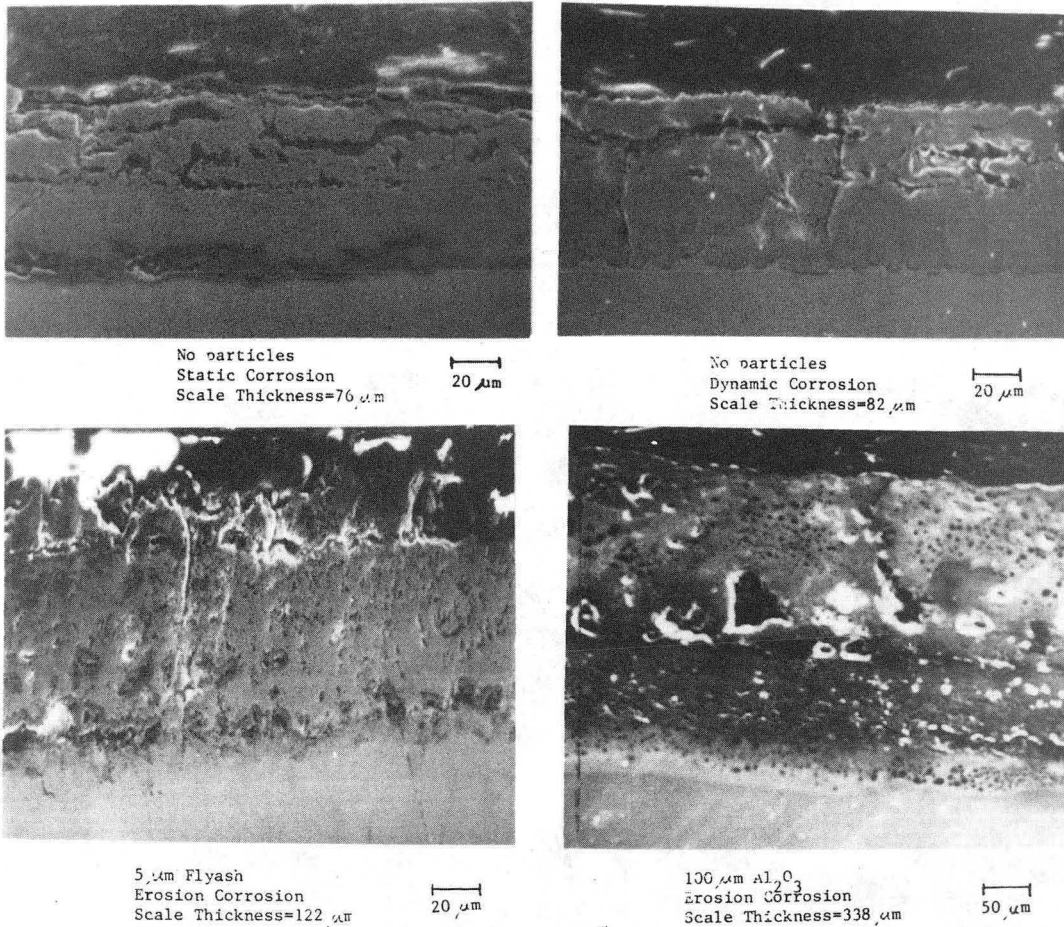
Fig. 7. Cross section of scales on 410SS from 100µm Al₂O₃ tests at 950°C.



2 1/4 Cr 1 Mo Steel
 Emersion Tester Temp. =850°C
 100µm Al₂O₃ Vel. =15m/s
 Methane-air =45°
 Time =30min.

XBB 841-98

Fig. 8. Cross section of scales on 2 1/4 Cr1Mo steel from 100µm Al₂O₃ tests at 850°C.



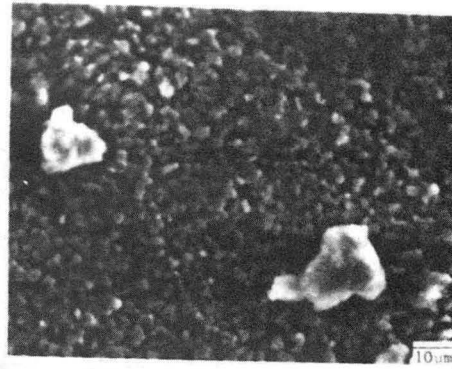
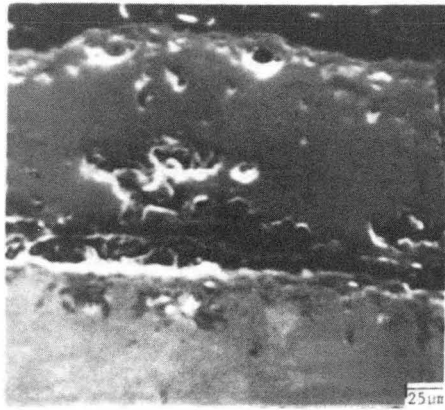
410SS

Emersion Tester
Methane-air
Time=30 min.

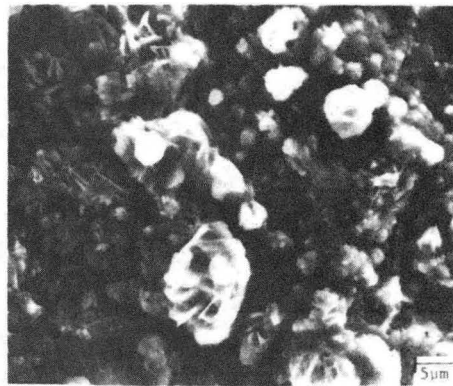
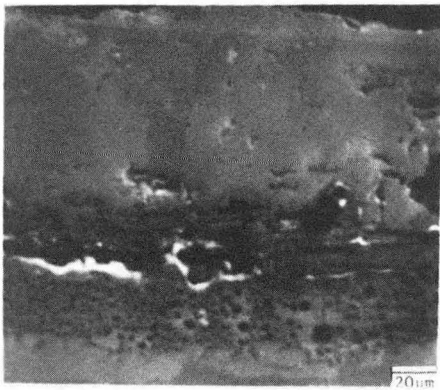
Temp.=950°C
Vel.=15mm/s
 $\alpha=45^\circ$

Fig. 9. Cross section of scales formed on 410SS at 950°C at different test conditions.

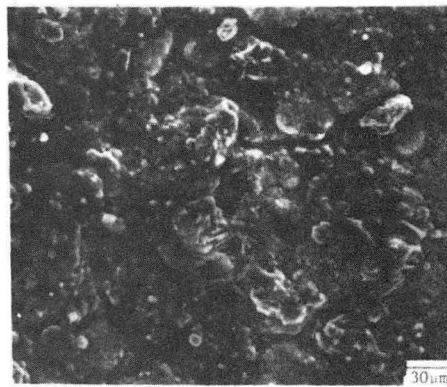
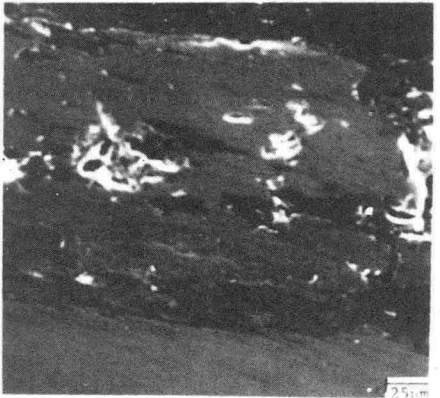
XBB 841-97



2 1/4 Cr 1 Mo Steel



9 Cr 1 Mo Steel

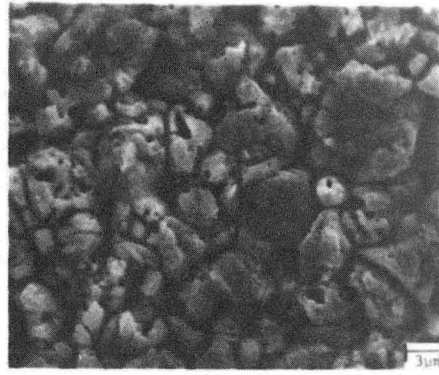
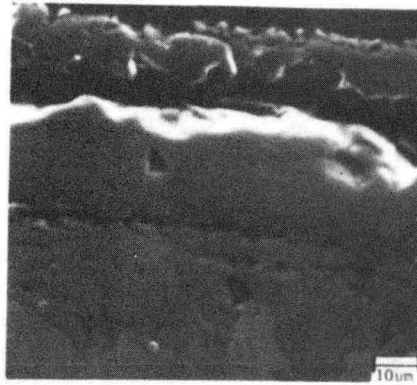


410 SS

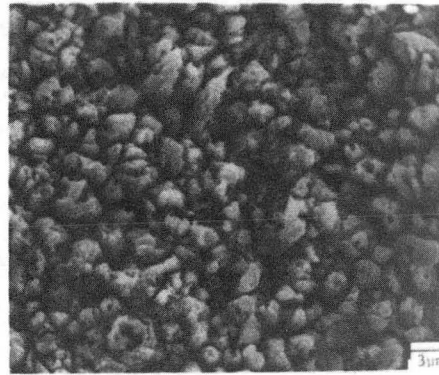
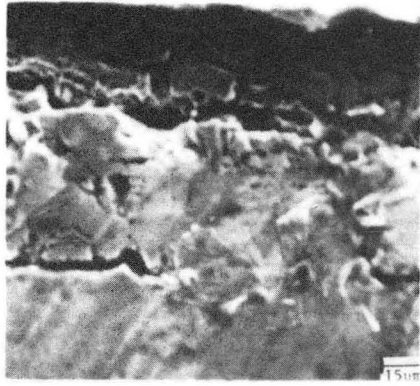
Emersion Tester	Temp. =850°C
Erosion-Corrosion	Vel. =15m/s
100µm Al ₂ O ₃	α =45°
Methane air	Time =30min.

Fig. 10. Cross section and surface morphology of scales of 2 1/4, 9 and 12Cr steels eroded-corroded at 850°C using 100µm Al₂O₃.

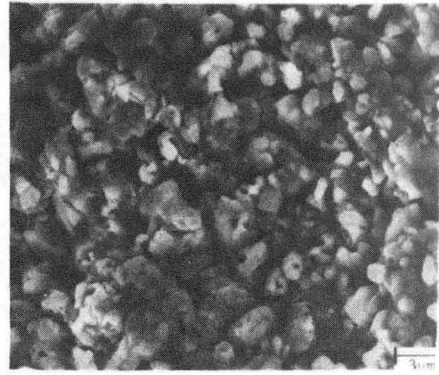
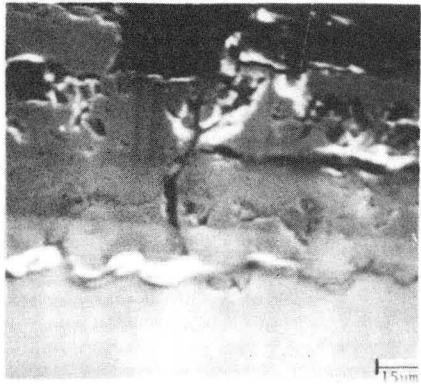
XBB 841-96



5 Cr 1/2 Mo Steel



9 Cr 1 Mo Steel

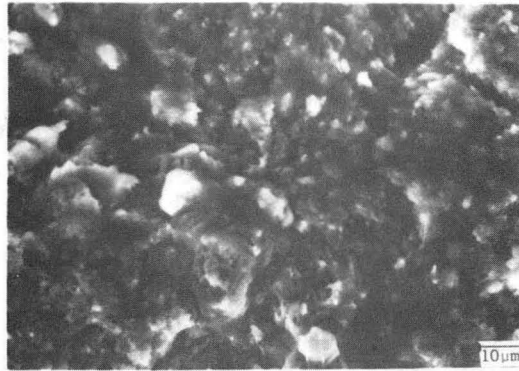


410 SS

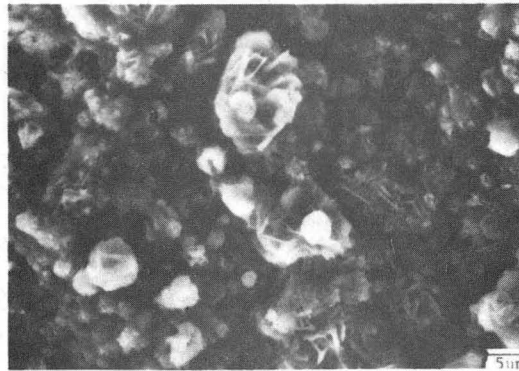
Emersion Tester	Temp. =950°C
Erosion-Corrosion	Vel. =15m/s
50µm Al ₂ O ₃	α =45°
Methane air	Time =30min.

Fig. 11. Cross section and surface morphology of scales of 5, 9 and 12Cr steels eroded-corroded at 950°C using 50µm Al₂O₃.

XBB 841-105



9 Cr 1 Mo Steel
Temp. =800°C



9 Cr 1 Mo Steel
Temp. =850°C

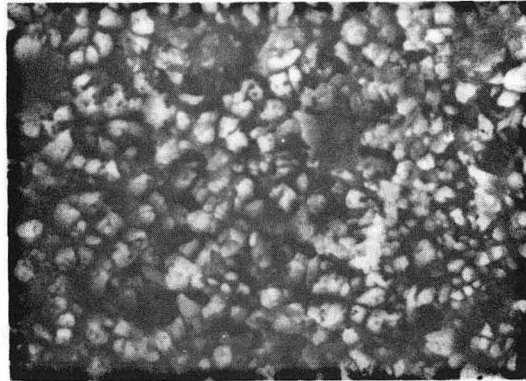


9 Cr 1/2 Mo Steel
Temp. =950°C

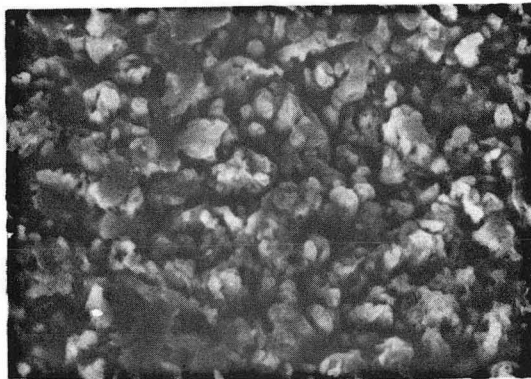
Emersion Tester	Methane-air
Erosion-Corrosion	Vel. =15m/s
100µm Al ₂ O ₃	α =45°

Fig. 12. Surface morphology of eroded-corroded 9Cr1Mo steel at three different test temperatures using 100µm Al₂O₃.

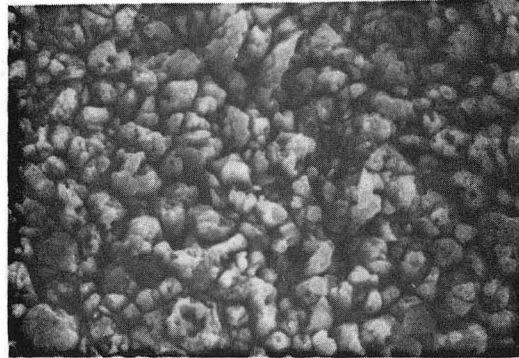
XBB 841-106



Temp. =850°C 3μm



Temp. =900°C 3μm



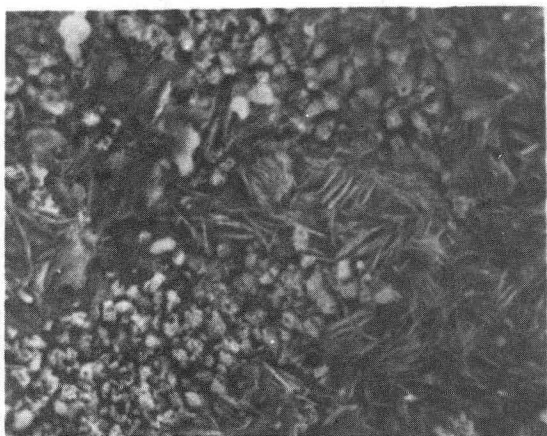
Temp. =950°C 3μm

9 Cr 1 Mo Steel

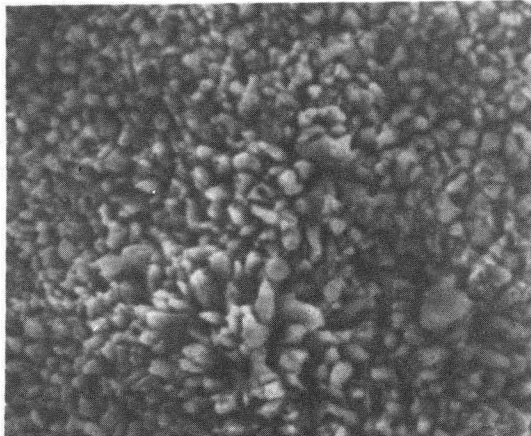
Emersion Tester	Methane-air
Erosion-Corrosion	Vel. =15m/s
50μm Al ₂ O ₃	α =45°

Fig. 13. Surface morphology of eroded-corroded 9Cr1Mo steel at three different test temperatures using 50μm Al₂O₃.

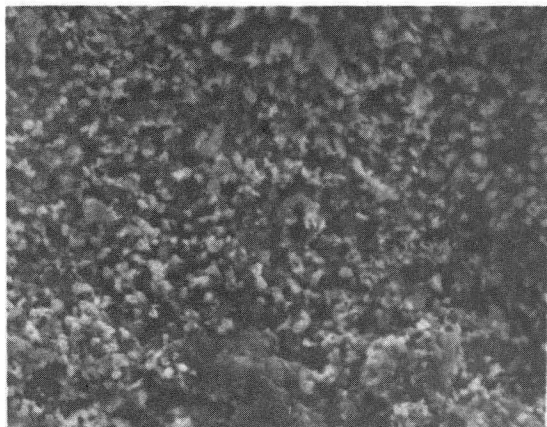
XBB 841-104



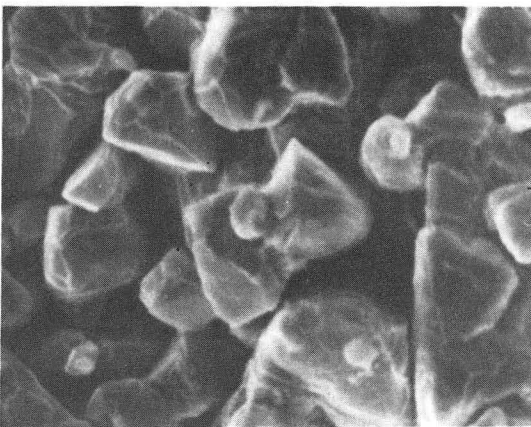
Corroded



Corroded



Eroded-Corroded



Eroded-Corroded



Temp. =850°C

410 SS

Temp. =950°C

Emersion Tester
5µm flyash
Methane-air

Vel. =15m/s
α =45°
Time =30min.

Fig. 14. Surface morphology of eroded-corroded 410SS at two test temperatures using 5µm flyash. XBB 841-107

DISTRIBUTION LIST

Wate Bakker
EPRI
3214 Hillview Avenue
P.O. Box 10412
Palo Alto, CA 94304

B.R. Banerjee
Ingersoll-Rand Company
P.O. Box 301
Princeton, NJ 08540

K.L. Baumert
Air Products & Chemicals, Inc.
P.O. Box 538
Allentown, PA 18105

S.M. Benford
NASA Lewis Research Center
21000 Brookpark Road
Cleveland, OH 41135

A.E. Biggs
Arco Chemicals
3801 W. Chester Pike
Newtown Square, PA 19073

R. Blickensderfer
Bureau of Mines
P.O. Box 70
Albany, OR 97321

R.A. Bradley, Manager
Fossil Energy Materials Program
Oak Ridge National Laboratory
P.O. Box X
Oak Ridge, TN 37830

Richard Brown
Materials Laboratory
Department of Chemical Engineering
University of Rhode Island
Kingston, RI 02881

DISTRIBUTION LIST cont'd

D.H. Buckley
NASA Lewis Research Center
21000 Brookpark Road
Cleveland, OH 41135

P.T. Carlson, Task Leader
Fossil Energy Materials Program
Oak Ridge National Laboratory
P.O. Box X
Oak Ridge, TN 37830

J. Carpenter
ECUT Program
Oak Ridge National Laboratory
P.O. Box X
Oak Ridge, TN 37830

J.P. Carr
Department of Energy, Office of Fossil Energy
FE-42 Mailstop 3222-GTN
Washington, DC 40525

Hans Conrad
Materials Engineering Department
North Carolina State University
Raleigh, NC 27659

P. Crook
Cabot Corporation
Technology Department
1020 W. Park Avenue
Kokomo, IN 46901

S.J. Dapkunas
Department of Energy, Office of Fossil Energy
Technical Coordination Staff FE-14
Mailstop C-156 GTN
Washington, DC 40525

DOE Technical Information Center
P.O. Box 62
Oak Ridge, TN 37830

W.A. Ellingson
Argonne National Laboratory
9700 South Cass Avenue
Argonne, IL 60439

DISTRIBUTION LIST cont'd

J. Gonzales
GTE
Chemical & Metallurgical Division
Hawes Street
Towanda, PA 18848

Å. Hammarsten
Teknikum
P.O. Box 534, S-751 21
Uppsala
SWEDEN

E. Haycock
Westhollow Research Center
Shell Development Company
P.O. Box 1380
Houston, TX 77001

J.M. Hobday
Department of Energy
Morgantown Energy Technology Center
P.O. Box 880
Morgantown, WV 26505

E.E. Hoffman, Manager
National Materials Program
Department of Energy
Oak Ridge Operations
P.O. Box E
Oak Ridge, TN 37830

J.A.C. Humphrey
Mechanical Engineering Department
University of California
Berkeley, CA 94720

I.M. Hutchings
University of Cambridge
Department of Metallurgy
Pembroke Street
Cambridge
ENGLAND

Sven Jansson
Stal-Laval Turbin AB
Finspong S-61220
SWEDEN

DISTRIBUTION LIST cont'd

R.R. Judkins
Fossil Energy Materials Program
Oak Ridge National Laboratory
P.O. Box X
Oak Ridge, TN 37830

M.K. Keshavan
Union Carbide Corporation
Coating Services Department
1500 Polco Street
Indianapolis, IN 46224

T. Kosel
University of Notre Dame
Dept. of Metallurgical Engineering
& Materials Science
Box E
Notre Dame, IN 46556

L. Lanier
FMC-Central Engineering Laboratory
1185 Coleman Avenue
Santa Clara, CA 95052

N.H. MacMillan
Pennsylvania State University
167 Materials Research Laboratory
University Park, PA 16802

P.K. Mehrotra
Kennemetal Inc.
1011 Old Salem Road
Greensburg, PA 15601

Ken Magee
Bingham-Williamette Co.
2800 N.W. Front Avenue
Portland, OR 97219

T. Mitchell
Case Western Reserve University
Department of Metallurgy
Cleveland, OH 44106

Fred Pettit
Dept. of Metallurgy & Materials Engineering
University of Pittsburgh
Pittsburgh, PA 15261

DISTRIBUTION LIST cont'd

R.A. Rapp
Metallurgical Engineering
116 W. 19th Avenue
The Ohio State University
Columbus, OH 43210

D.A. Rigney
Metallurgical Engineering
116 W. 19th Avenue
The Ohio State University
Columbus, OH 43210

A.W. Ruff
Metallurgy Division
National Bureau of Standards
B-266 Materials
Washington, DC 20234

Alberto Sagüés
IMMR - University of Kentucky
763 Anderson Hall
Lexington, KY 40506

Gordon Sargent
University of Notre Dame
Dept. of Metallurgical Engineering & Materials Science
Box E
Notre Dame, IN 46556

Paul Shewmon
Dept. of Metallurgical Engineering
116 W. 19th Avenue
Columbus, OH 43210

Gerry Sorell
EXXON Research & Engineering Company
P.O. Box 101
Florham Park, NJ 07932

John Stringer
University of California
Lawrence Berkeley Laboratory
Mailstop 62/203
Berkeley, CA 94720

Widen Tabakoff
Dept. of Aerospace Engineering
University of Cincinnati
Cincinnati, OH 45221

DISTRIBUTION LIST cont'd

Edward Vesely
IITRI
10 West 35th Street
Chicato, IL 60616

J.J. Wert
Metallurgy Department
Vanderbilt University
P.O. Box 1621, Sta. B
Nashville, TN 37235

J.C. Williams
Dept. of Metallurgy & Materials Science
Carnegie-Mellon University
Schenley Park
Pittsburgh, PA 15213

S. Wolf
Department of Energy
Basic Energy Sciences Office
Division of Materials Sciences
Washington, DC 20545

Ian Wright
Materials Science Division
Battelle Memorial Institute
505 King Avenue
Columbus, OH 43201

C.S. Yust
Metals and Ceramics Division
Oak Ridge National Laboratory
P.O. Box X
Oak Ridge, TN 37830

This report was done with support from the Department of Energy. Any conclusions or opinions expressed in this report represent solely those of the author(s) and not necessarily those of The Regents of the University of California, the Lawrence Berkeley Laboratory or the Department of Energy.

Reference to a company or product name does not imply approval or recommendation of the product by the University of California or the U.S. Department of Energy to the exclusion of others that may be suitable.

TECHNICAL INFORMATION DEPARTMENT
LAWRENCE BERKELEY LABORATORY
UNIVERSITY OF CALIFORNIA
BERKELEY, CALIFORNIA 94720